Nanoscale

Accepted Manuscript

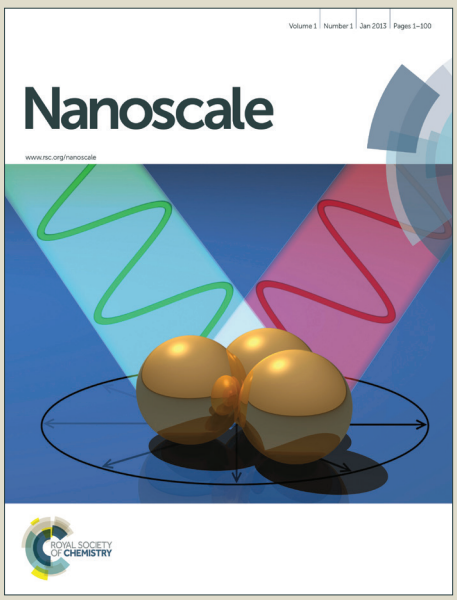

ROYAL SOCIETY OF CHEMISTRY

www.rsc.org/nanoscale

Cite this: DOI: 10.1039/c0xx00000x

www.rsc.org/xxxxxx

ARTICLE TYPE

Layer Speciation and Electronic Structure Investigation of Freestanding Hexagonal Boron Nitride Nanosheets

Jian Wang[a‡], Zhiqiang Wang[b‡], Hyunjin Cho[c], Myung Jong Kim[c], T.K. Sham[b,d], Xuhui Sun[d,e]*

Received (in XXX, XXX) Xth XXXXXXXXX 20XX, Accepted Xth XXXXXXXXX 20XX
DOI: 10.1039/b000000x

Chemical imaging, thickness mapping, layer speciation and polarization dependence have been performed on single and multilayered (up to three layers and trilayer nanosheets overlapping to form 6 and 9 layers) hexagonal boron nitride (hBN) nanosheets by scanning transmission X-ray microscopy. Spatially-resolved XANES directly from freestanding regions of different layers have been extracted and compared with sample normal and 30° tilted configurations. Notably a double feature σ* excitonic state and a stable high energy σ* state were observed at the boron site in addition to the intense π* excitonic state. The boron projected σ* DOS, especially the first σ* exciton, is sensitive to surface modification, particularly in the single layer hBN nanosheet which shows more significant detectable contaminants and defects such as tri-coordinated boron/nitrogen oxide. Nitrogen site has shown very weak or no excitonic character. The distinct excitonic effect on boron and nitrogen was interpreted to the partly ionic state of hBN. Bulk XANES of hBN nanosheets was also measured to confirm the spectro-microscopic STXM result. Finally, the unoccupied electronic structure of hBN and graphene were compared.

Keywords: hBN, nanosheets, STXM, XANES, exciton, polarization.

Introduction

Nanosheets of hexagonal boron nitride (hBN) exhibit a honey cone structure similar to that of graphene, with sp^2 hybridized boron and nitrogen atoms alternately bonded in the basal plane, as illustrated in Fig. 1.This unique structure leads to some excellent properties,[1-4] such as high chemical and thermal stabilities, enhanced thermal and electrical conductivity in the basal plane, and versatile doping capabilities. Thus hBN nanosheets have attracted increasing attentions in many fields and been used in various applications, such as dielectric layers/substrates[5] and thermal management[6] for electronic devices (particularly ideal for graphene devices), deep UV light emitters,[7,8] and functional coatings.[9] However, unlike graphene, the partly ionic B-N bond in hBN reduces electron-delocalization and creates a large band gap (~6 eV) in the ultraviolet (UV), making hBN a remarkably wide band gap semiconductor. Furthermore, fascinating effects and phenomena for the single layer hBN are being discovered or predicted, such as an unusual nonlinear electromechanical effect.[10] Therefore, high quality and large area of hBN nanosheets are extremely valuable, and an in depth understanding of the morphology and the electronic structure of individual hBN nanosheets will be of great importance in the development of sophisticated technologies.

For hBN nanosheets, local structure/geometry varies among individual hBN nanosheets or even within a single sheet, and defects and impurities may also exist in the sample, so an accurate characterization demands microscopic measurements and direct probing the properties on a single hBN nanosheet. Scanning transmission X-ray microscopy (STXM) using a nanoscale focused soft X-ray beam provides an excellent combination of microscopic characterization and chemical/electronic structure speciation via X-ray absorption near edge structure (XANES) spectroscopy for individual nanomaterials. STXM has been successfully applied to studies of graphene etc. nanomaterials for electronic structure investigation and chemical/morphology imaging.[11-16] Furthermore, as hBN nanosheets are highly polarized, identifying a local flat sample region with uniform polarization effect is critical and the polarized STXM with the help from the Elliptically Polarizing Undulator (EPU) as the X-ray source of the beamline is well suited for this purpose. In this letter, we report an application of STXM in the characterization of a deliberately selected sample region of single and multilayered hBN nanosheets with respect to layer speciation/thickness determination and the polarization and thickness effects. Spatially-resolved and polarized XANES directly from local regions of interest on the nanosheets were obtained. In addition, XANES spectroscopy of hBN nanosheets in the bulk was also measured to compare with STXM results to confirm the polarization effect observed by STXM and evaluate the possible substrate effect. Since the bulk spectroscopy was conducted over a large sampling area with typical beam spot size of 100×100 μm^2, it provided information on the average of all possible morphologies, orientations and sample thickness. Finally, we briefly compare the XANES (i.e. unoccupied electronic structure) of hBN with that of graphene to elucidate the similarities and origins of the corresponding spectroscopic features. We believe such a comparison and conclusions thus obtained will be generally applicable for other similar systems.

Experimental

Synthesis of hBN nanosheets

High quality stoichiometric hBN nanosheets were prepared adopting low pressure chemical vapor deposition (LPCVD).[17] Nickel foil (0.020mm thick, 99%, The Nilaco Corporation) was employed as the metal catalyst. In order to planarize the surface and to remove contaminations on the nickel foil, electrochemical polishing method was used, and the Ni foil was sequentially cleaned by acetone, isopropyl alcohol (IPA) and deionized water. Then, the nickel foil was placed in a 2-inch quartz tube in CVD apparatus and annealed under atmospheric pressure of hydrogen gas for 30 min at 1100 ^{o}C for surface reduction and clean, and thus increase the grain size of the nickel foil. For the growth, 0.3 sccm of Borazine ($B_3N_3H_6$, precursor for hBN) in conjunction with 100 sccm of hydrogen gas was introduced into the quartz tube furnace for 10 min at 1100 ^{o}C under high vacuum condition achieved with a turbo pump. Thus, the operating pressure for the growth process was as low as 6 mTorr. The flow of Borazine in the CVD apparatus was turned off after the growth process, and the synthesized hBN sample in the quartz tube was cooled down rapidly to room temperature at the flow rate of 300 sccm of hydrogen. Ni foil was removed by dissolving in $FeCl_3$ aqueous solution, and the hBN nanosheets were rinsed in deionized water. The floating hBN nanosheets were transferred onto a lacey carbon TEM grid for further characterization.

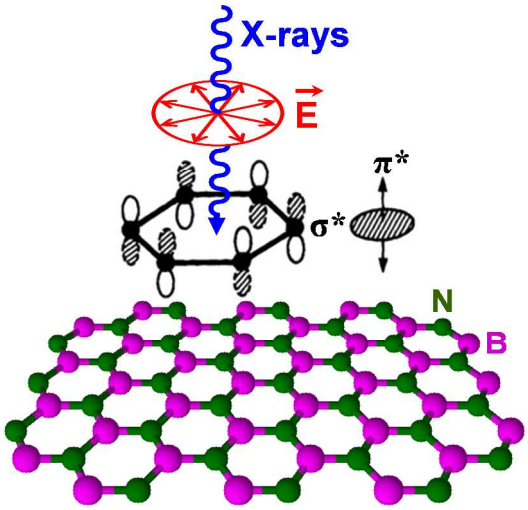

Fig. 1 Structure of an hBN single sheet and illustration of the in-plane circularly polarized X-rays shining on the sample in STXM.

Characterization

hBN nanosheets supported by TEM grid were directly used for STXM measurement. STXM measurements were conducted at the SM beamline of the Canadian Light Source (CLS).[18] In-plane circularly polarized light from EPU was used to probe the polarization effect, as illustrated in Fig. 1. In STXM, the monochromatic X-ray beam is focused by a Fresnel zone plate to a ~30 nm spot on the sample, and the sample is raster-scanned with synchronized detection of transmitted X-rays to generate image sequences (stacks) over a range of photon energies.[11] Image stacks at the B K-edge and N K-edge were acquired at the same selected region where the well-defined hBN nanosheets and some empty areas for normalization were found. STXM data were analyzed by freeware aXis2000 (http://unicorn.mcmaster.ca/aXis2000.html). Briefly, B K-edge and N K-edge image stacks were appended, and then aligned and converted to optical density (OD, i.e. absorbance). XANES spectra for different regions of interest were extracted from the combined image stack using image masks. The hBN reference spectrum, as shown in Fig. 2a, was obtained by averaging all measured hBN nanosheet regions and was quantitatively scaled to represent 1 nm thick XANES by fitting the spectrum to the theoretical elemental X-ray absorption profile of BN for 1 nm thick material with known density of 2.1 g/cm^3, calculated based on the photo-absorption cross-sections and atomic scattering factors of elements reported in the literature.[20] Quantitative chemical imaging/thickness mapping was then conducted by fitting the stack with the reference spectrum of hBN and the featureless X-ray absorption of lacey carbon at B K-edge and N K-edge. A color composite image was created by combining individual component maps with the image intensity rescaled for better contrast. More details of the STXM experimental and data analysis procedures can be found elsewhere.[11,21-23]

Bulk XANES spectroscopy of hBN nanosheets was conducted at the SGM (N K-edge) and PGM (B K-edge) beamlines of CLS with typical beam spot size of 100×100 μm^2. The as-prepared hBN nanosheets on Ni foil was attached to the sample holder by conductive carbon tape. XANES was recorded in the surface sensitive total electron yield (TEY) by measuring the sample current, and in the bulk sensitive fluorescence yield (FLY) and partial fluorescence yield (PFY) using silicon drift detector (SDD) with the detection window set at the N Kα fluorescence. XANES data were first normalized to the incident photon flux I_0 measured with a refreshed gold mesh prior to the measurement, and then were normalized to the edge-jump.

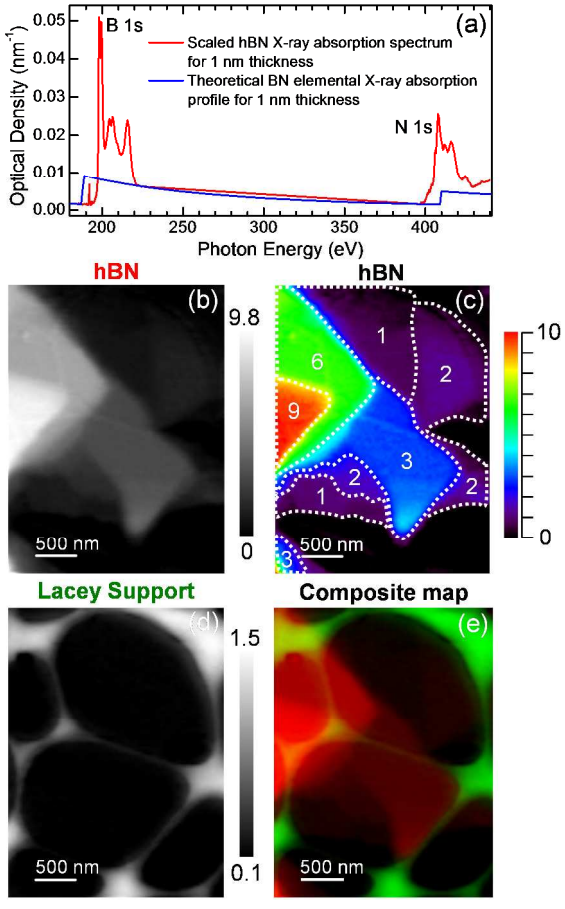

Fig. 2 STXM characterization of the hBN nanosheets on a holey lacey carbon film coated TEM grid, (a) linearly scaled reference spectrum of hBN (spectrum scaled to the calculated BN elemental X-ray absorption profile for 1 nm thick material, BN density is 2.1 g/cm^3); (b) hBN

thickness map in grey colour scheme, and (c) in rainbow color scheme, the vertical scales on the right represent the materials thickness in nm, the enclosed white dotted lines indicate the regions of different hBN layers, labelled with the number of layers; (d) map of the lacey carbon support, the grey vertical scale on the right represents the intensity ratio to the reference spectrum in arbitrary unit; (e) color composite map, red: hBN, green: lacey carbon support.

Results and Discussion

A well-defined sample region of hBN nanosheets supported on a holey lacey carbon TEM grid was selected and characterized by STXM image stacks at the B K-edge and N K-edge. The quantitative thickness map of the hBN nanosheets derived by stack fitting is displayed in Fig. 2b. The nanosheets show a multilayered structure with the STXM determined thickness variation from about 0.3 nm to 9.8 nm. The highest thickness region is shown in the middle left (lightest contrast region). For a clearer view of the layered structure, the same image was displayed in a linearly scaled rainbow color scheme, as shown in Fig. 2c. Based on the thickness variation and distribution, the nanosheets can be categorized into several regions with different thickness, as shown by the enclosed white dotted lines labelled with the number of layers in Fig. 2c. For the thinnest regions (labelled 1), the thickness is primarily under 1 nm with a median thickness about 0.7 nm, which is considered as a single layer of hBN nanosheet. The STXM determined thickness of a single layer hBN nanosheet seems much higher than the actual thickness of 0.33 nm for a single layer hBN.[24] There are a few possible reasons for the discrepancy, such as optical density measurement error and the methodology error between the thickness calculated from photo-absorption and direct thickness measurements by AFM and TEM, for the ultrathin sub-nanometer sample thickness. A TEM characterization of the similarly prepared sample was reported in our previous work, which demonstrated the thickness of the hBN nanosheets was typically from single to three layers and layer by layer growth had been achieved, with controlled gas flow rate and ratio in the LPCVD synthesis.[17] Therefore we have great confidence that the thinnest region in this work should be singly layer hBN. Our latest work for the single layer graphene has obtained a smallest optical density of 0.007 for the carbon edge jump, which is quite comparable to this work for the single layer hBN,[25] but still showing similar degree of error. This systematic discrepancy implies a possible methodology error in STXM thickness determination for ultrathin sub-nanometer sample, and our studies could provide useful calibration information. It is also worth noting that hBN can form nanoscale surface domains/islands/patches, as clearly seen by TEM in our previous work,[17] however most of which are smaller than the STXM spatial resolution of ~30 nm, while only some large domains can actually be seen by STXM, as to be addressed below. These domains of varied thickness will inadvertently increase the nominal thickness of the single layer hBN if their number is significant. Apart from the single layer regions, other regions on Fig. 2c display thickness of about integer folds of the single layer, namely bilayer, trilayer, 6 layers and 9 layers. These are due to a multilayered structure up to three layers (consistent with the TEM characterization of a similar sample[17]) and trilayer nanosheets overlapping to form 6 and 9 layers because of inefficient dispersion during sample preparation. Fig. 2d shows the morphology of the lacey carbon support in the measured sample region also obtained by stack fitting. Because lacey carbon does not contain boron and nitrogen, it can be mapped out accurately. Fig. 2e presents a colour composite image of the hBN nanosheets and the lacey carbon support with image intensity rescaled in each color channel for a better view of all the components.

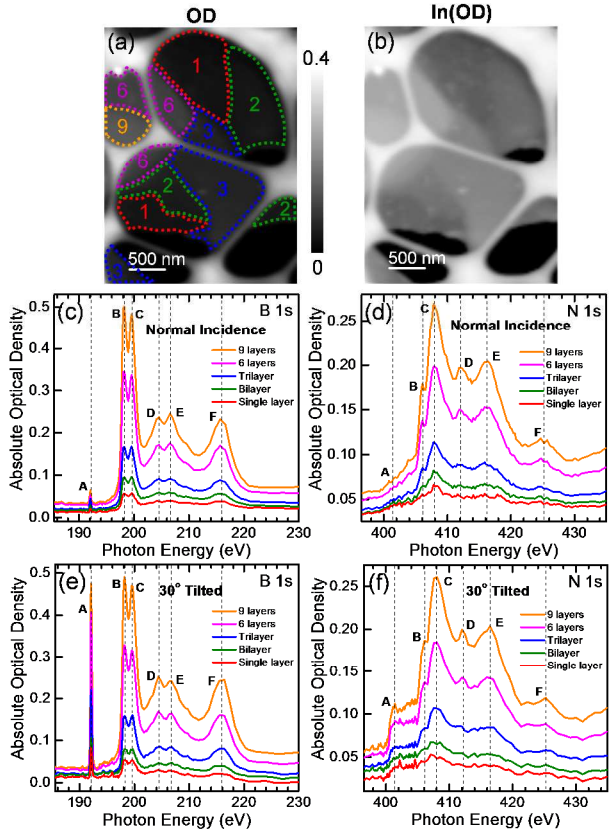

Fig. 3 STXM spatially-resolved XANES spectra of hBN nanosheets, (a) STXM optical density image of the measured sample region (the image was averaged from all stack images at the B and N K-edges), the enclosed color dotted lines indicate the regions of interest on hBN nanosheets for extracting XANES spectra, red: single layer, green: bilayer, blue: trilayer, pink: 6 layers, and orange: 9 layers, the vertical scale on the right represents the averaged optical density; (b) the natural logarithm image of (a) for better view of the thin regions and surface domains/islands/patches; (c) and (d) absolute optical density XANES spectra with normal incidence of the X-ray beam, (e) and (f) absolute optical density XANES spectra with the sample tilted by 30° with respect to the incident beam, at the B and N K-edge respectively from the selected regions of interest in (a), all vertical dashed lines and letters in the spectra indicate the spectral regions of interest.

In order to investigate the electronic structure and any chemical interactions within the hBN nanosheets, spatially-resolved XANES spectra from individual multiplayer regions have been extracted. Fig. 3a shows an OD image of the sample region of interest, obtained by averaging all stack images at the B K-edge and N K-edge. Based on previous chemical imaging/thickness mapping, regions of single layer, bilayer, trilayer, 6 layers and 9 layers have been selected at the freestanding nanosheet regions, avoiding any contribution from the lacey carbon support, as outlined by the enclosed color dotted lines in Fig. 3a. For a better view of the thin regions, the OD image was taken in natural logarithm, displayed in Fig. 3b where all individual thin layers can be clearly resolved and spatially identified. Furthermore, on the nanosheets there are a number of blurred bright spots/patches, albeit weak in intensity, which can still be resolved by STXM. These nanoscale spots/patches turned out to be hBN surface domains/islands after carefully analyzing their spectroscopy in the image stacks. Fig. 3c and 3d present the local XANES

spectroscopy at the B K-edge and N K-edge respectively, obtained from the selected regions of interest in Fig. 3a with normal incidence of the X-ray beam. Fig. 3e and 3f show the same spectra with the sample tilted by 30° with respect to the incident beam. Since these spectra are in absolute OD scale, their overall intensity is linearly proportional to the thickness of the nanosheets, highly consistent with the layer speciation in Fig. 2, demonstrating the quantitative capability of X-ray absorption in STXM. Fig. S1a and S1b in the supplementary information are the normalized spectra of Fig. 3c and 3d, respectively, in order to reveal the electronic structure insights without the interference from the thickness effect. The normalization at the B K-edge is to scale the edge-jump at 185 and 230 eV to unity and at 395 and 430 eV for the N K-edge.

Looking at the B K-edge XANES in Fig. 3c, 3e and Fig. S1a, there are six features clearly resolved, numbered from A to F, which detail the structure information of the hBN framework. Specifically, feature A (192.1 eV) is the well-known $\pi^*(2p_z)$ resonance of hBN.[26] A highly flat hBN nanosheet should have a very week π* like the normal beam incidence spectra because the electric vector of the in-plane circularly polarized X-ray beam is orthogonal to it and therefore not able to excite the π*,[11] as illustrated in Fig. 1. The weakly visible π* must arise from regions that are not perfectly flat likely due to wrinkle/folding of the nanosheets, the less crystalline surface domains/islands, and a slight misalignment of the sample with respect to the incident beam. When the sample is tilted by 30° with respect to the incident beam, the π* peak intensity increases strikingly, as shown in Fig. 3e. Higher energy features B to F are all assigned to σ* resonance of hBN, which are readily excited by the in-plane polarized beam to show pronounced intensities. More explicitly, from the molecular orbital (MO) perspective, the intense double feature B (198.2 eV) and C (199.6 eV) are due to localized $\sigma^*(2p_x, 2p_y)$ antibonding between boron and nitrogen; or in the band theory, they could be assigned to the transitions to the maximum density of states (DOS) at the L/M and Γ point of the first Brillouin zone (BZ) of hBN, respectively.[27,28] The sharp intensity suggests their excitonic nature, namely a stable state of a core hole coupled with a bound excited electron (i.e. electron-hole pair).[29] Another pair of features, D (204.4 eV) and E (206.6 eV), displaying similar profile as feature B and C, can be assigned to moderate range $\sigma^*(2p_x, 2p_y)$ involving more boron and nitrogen atoms, or a maximum DOS along ΓM or ΓK direction of the BZ in the band theory.[27,28] Finally feature F (215.9 eV) is considered as a large range σ* antibonding state involving the six-membered ring framework, and interestingly this is a surprisingly stable state on boron at such a high energy well above the ionization potential that is typically around the first σ* double feature.

After normalization to the same edge-jump and zooming in the energy region between 191 and 197 eV for the normal incidence in Fig. S1c in the supplementary information, we can see some systematic changes for the spectra of different layers: (1) a weak contaminant feature at ~194 eV due to tri-coordinated boron oxide environment[30-33] and another feature at ~196 eV hardly distinguishable from the noisy background are more clearly seen in the single layer, and their intensity gradually decreases with increasing layer number to 9 layers. This observation indicates that the thinner the layer, the more dominant the surface contaminants and defects; (2) the intensity ratio of σ*(B, C) to π*(A) substantially increases from the single layer to 9 layers, as shown in Fig. S1d, which indicates a better crystallinity (or flatness) and less significant from the surface contaminants in thicker layers; (3) the intensity ratio of the excitonic feature B to C slightly increases with the layer number, indicating that feature B is sensitive to the surface and framework modification, as was observed in graphene. The 30° tilted spectra in Fig. 3e appear to show more pronounced contaminant features at 194 and 196 eV, similar behavior as the hBN π* feature, which suggests the contaminant elements are inserted into the hBN framework, consistent with a tri-coordinated boron oxide environment. Although the surface contaminants are marginally visible in the B K-edge, their amount is too small to be clearly identified in the C and O K-edges, as shown in Fig. S2 in the supplementary information.

The N K-edge XANES of hBN, shown in Fig. 3d, 3f and Fig. S1b, display similar features as the B K-edge. Considering the equivalent geometry of nitrogen and boron in hBN, the feature assignment follows the same as the B K-edge. The π* feature A is located at ~401.2 eV in 30° tilted spectra,[34] but it is too weak to be observed in the normal incidence due to the polarization effect. Unlike boron, nitrogen π* and σ* feature B (406.0 eV) only show weak excitonic nature, and σ* feature C (408.0 eV) does not show typical excitonic behavior at all because in ionic or polar compounds, due to different Coulomb interaction and screening efficiency, excitonic states are more strongly bound at the cation than at the anion site.[29,35] Therefore the excited π* and σ* states on the nitrogen site are either very unstable resulting in weak spectral intensity or the lifetime is reduced inducing broadened spectrum. The other pair of σ* features, D (412.1 eV) and E (416.3 eV), show similar intensity trend as feature B and C. Lastly feature F (424.9 eV) is considerably weaker than its boron counterpart. After normalization in Fig. S1b, together with the steady increase of the intensity ratio of σ*(B, C) to π*(A) from single layer to 9 layers in Fig. S1d, likewise the B K-edge, the same surface and bulk behavior can be concluded for the N K-edge. The 30° tilted spectra in Fig. 3f also show more evident contaminant features at 402.2 and 404.6 eV, same behavior as the hBN π* feature A, implying that the contaminant elements are inserted into the hBN framework, consistent with a tri-coordinated nitrogen oxide environment.

To complement the spectro-microscopic STXM characterization, bulk XANES spectroscopy of hBN nanosheets was also acquired. Fig. 4a and 4b compare normalized XANES spectra obtained by surface sensitive TEY and the bulk sensitive FLY/PFY compared with the STXM result at the B K-edge and N K-edge with normal incidence and 30° tilted, respectively. The B K-edge shows more dramatic difference. In general, bulk XANES shows much more intense π* than STXM normal incidence, while STXM shows overall higher σ* intensities; these are mainly because (1) bulk measurements have all possible morphologies/orientations and thickness of the sample (random sample with perhaps some texture effects) and they were conducted with linearly polarized light, and (2) microscopically flat nanosheets in STXM have different polarization response. More interestingly, the TEY XANES shows drastically reduced excitonic feature B compared to FLY and STXM; this is a good example to confirm the conclusion obtained from STXM that feature B is very sensitive to the surface modification such as contamination, adsorption and functionalization, so that the excitonic state cannot be effectively formed or is quenched. The N K-edge shows insignificant difference, only with the bulk XANES π* feature slightly more pronounced than the normal incidence STXM. Unlike STXM, the bulk spectroscopy at the B and N K-edges essentially does not show any contaminants or is insensitive to the trace amount of

them, which suggests trace amount of surface contaminants is still existent and detectable by microscopic STXM characterization although the sample is pure as viewed macroscopically.

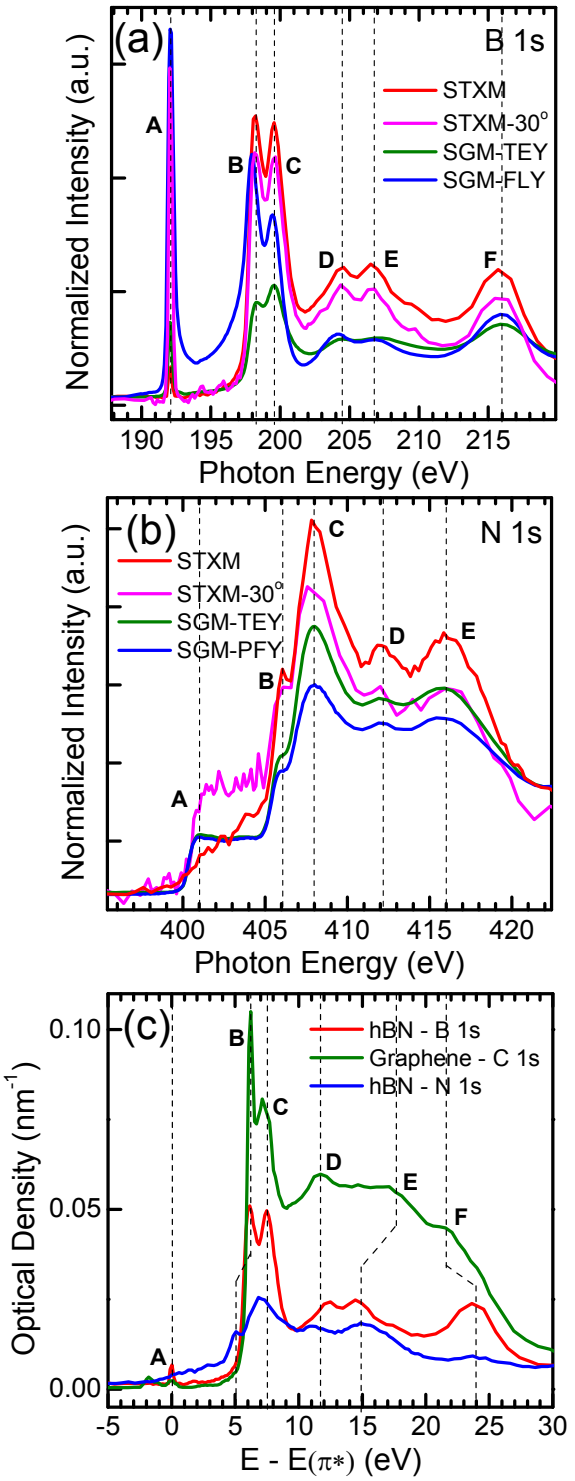

Fig. 4 (a) B K-edge, and (b) N K-edge normalized XANES spectra of hBN nanosheets obtained by normal incidence and 30° tilted STXM compared with bulk spectroscopic measurements recorded in TEY and FLY/PFY; (c) comparison of the unoccupied electronic structure between hBN and graphene as probed at B 1s, N 1s and C 1s with the π* feature set at a common point. All vertical dashed lines and letters in the spectra indicate the spectral regions of interest.

Finally, it is interesting to compare the electronic structure of the two similar systems, hBN and graphene. Fig. 4c compares the linearly scaled XANES spectra (OD/nm) between hBN (Fig. 2a) and graphene probed at B 1s, N 1s and C 1s[11] with the π* feature set at a common point. Not surprisingly, their spectroscopic features match well, suggesting similarities in origins of these features. Other than that, graphene has much higher edge-jump and overall intensities than hBN because there is twice number of carbon atoms compared to boron or nitrogen for the same nanosheet thickness. In addition, graphene shows a much stronger and sharper excitonic state for the first σ* peak than hBN, consistent with its higher conductivity and smaller dielectric constant, and longer lifetime of the excitonic state. In spite of that, boron does show good excitonic character with a double σ* excitonic state in hBN nanosheets. Although hBN excitonic states are weaker than that of graphene, they show more degenerated states than graphene. As many properties of insulating and semiconductor materials are strongly related to excitons, especially for low-dimensional systems,[36] a good understanding of the exciton and the factors affecting them, such as ionic state, surface modification, as elucidated in this work, will be very valuable to guide the design and engineering of novel materials.

Conclusions

In summary, STXM has been used to track the morphology and electronic properties of multilayered freestanding hBN nanosheets. Chemical imaging, thickness determination, layer speciation, and polarization dependence have been performed on a selected sample region with hBN nanosheet thickness varying from a single layer to 9 layers. In addition, spatially resolved XANES of different layers on the nanosheets have been extracted and compared with beam normal incidence and sample 30° tilted. A double feature σ* excitonic state (198 - 200 eV) and a stable high energy σ* state (216 eV) were observed at the boron site in addition to the intense π* excitonic state. Furthermore, the boron projected σ* DOS, especially the first excitonic feature, is sensitive to surface perturbation such as contamination, adsorption and functionalization, particularly in the single layer hBN nanosheet which shows more significant detectable contaminants and defects, such as tri-coordinated boron/nitrogen oxide. Nitrogen site on the other hand shows very weak or no excitonic character. The distinct excitonic effect on boron and nitrogen was interpreted in terms of the partly ionic character of the B-N bond in hBN. Bulk XANES of hBN nanosheets powder was measured at B K-edge and N K-edge to confirm the spectro-microscopic STXM results and the strong polarization effect observed in STXM. Finally, the electronic structure of hBN and graphene was compared, and differences and similarities were addressed.

Acknowledgments

We thank Dr. Chithra Karunakaran, Dr. James J. Dynes and Yingshen Lu for assistance at the SM beamline, and Dr. Tom Regier at the SGM beamline. The Canadian Light Source is funded by the Canada Foundation for Innovation, the Natural Sciences and Engineering Research Council of Canada, the National Research Council Canada, the Canadian Institutes of Health Research, the Government of Saskatchewan, Western

Economic Diversification Canada, and the University of Saskatchewan. The work was supported by the National Basic Research Program of China (973 Program) (Grant No. 2010CB934500), Natural Science Foundation of China (NSFC) (Grant No. 91333112**,** U1432249), the Priority Academic Program Development of Jiangsu Higher Education Institutions. This is also a project supported by the Fund for Innovative Research Teams of Jiangsu Higher Education Institutions. The work at KIST was supported by the Korea Institute of Science and Technology Institutional Program and the Graphene Materials/Components Development Project funded by the Ministry of Trade, Industry, and Energy (MOTIE), Republic of Korea.

Notes and references

[a] Canadian Light Source Inc., University of Saskatchewan, Saskatoon, SK S7N 2V3, Canada.
[b] Department of Chemistry, University of Western Ontario, London, ON N6A 5B7, Canada
[c] Soft Innovative Materials Research Center, Korea Institute of Science and Technology, Wanju-gun, Jeollabuk-do 565-905, South Korea
[d] Soochow University-Western University Centre for Synchrotron Radiation Research
[e] Institute of Functional Nano & Soft Materials (FUNSOM) and Collaborative Innovation Center of Suzhou Nano Science & Technology, Soochow University, Suzhou, Jiangsu, 215123, China
* Email: xhsun@suda.edu.cn
‡ Equal contribution to this work

(1) Lipp, A.; Schwetz, K. A.; Hunold, K. *J. Eur. Ceram. Soc.* **1989**, *5*, 3-9.
(2) Paine, R. T.; Narula, C. K. *Chem. Rev.* **1990**, *90*, 73-91.
(3) Kho, J.-G.; Moon, K.-T.; Kim, J.-H.; Kim, D.-P. *J. Am. Ceram. Soc.* **2000**, *83*, 2681-2683.
(4) Chen, Y.; Zou, J.; Campbell, S. J.; Le Caer, G. *Appl. Phys. Lett.* **2004**, *84*, 2430-2432.
(5) Kim, K. K.; Hsu, A.; Jia, X.; Kim, S. M.; Shi, Y.; Dresselhaus, M.; Palacios, T.; Kong, J. *ACS Nano* **2012**, *6*, 8583-8590.
(6) Chang, C. W.; Fennimore, A. M.; Afanasiev, A.; Okawa, D.; Ikuno, T.; Garcia, H.; Li, D.; Majumdar, A.; Zettl, A. *Phys. Rev. Lett.* **2006**, *97*, 085901.
(7) Watanabe, K.; Taniguchi, T.; Kanda, H. *Nat. Mater.* **2004**, *3*, 404-409.
(8) Kubota, Y.; Watanabe, K.; Tsuda, O.; Taniguchi, T. *Science* **2007**, *317*, 932-934.
(9) Pakdel, A.; Zhi, C.; Bando, Y.; Nakayama, T.; Golberg, D. *ACS Nano* **2011**, *5*, 6507-6515.
(10) Naumov, I.; Bratkovsky, A. M.; Ranjan, V. *Phys. Rev. Lett.* **2009**, *102*, 217601.
(11) Zhou, J. G.; Wang, J.; Sun, C. L.; Maley, J. M.; Sammynaiken, R.; Sham, T. K.; Pong, W. F. *J. Mater. Chem.* **2011**, *21*, 14622-14630.
(12) Sun, C.-L.; Chang, C.-T.; Lee, H.-H.; Zhou, J.; Wang, J.; Sham, T.-K.; Pong, W.-F. *ACS Nano* **2011**, *5*, 7788-7795.
(13) Schultz, B. J.; Patridge, C. J.; Lee, V.; Jaye, C.; Lysaght, P. S.; Smith, C.; Barnett, J.; Fischer, D. A.; Prendergast, D.; Banerjee, S. *Nat. Commun.* **2011**, *2*, 372.
(14) Wang, J.; Zhou, J.; Hu, Y.; Regier, T. *Energy Environ. Sci.* **2013**, *6*, 926-934.
(15) Bai, L.; Liu, J.; Zhao, G.; Gao, J.; Sun, X.; Zhong, J. *Appl. Phys. Lett.* **2013**, *103*.
(16) Zhou, C.; Wang, J.; Szpunar, J. A. *Chem. Commun.* **2014**, *50*, 2282-2285.
(17) Kim, S.-K.; Cho, H.; Kim, M. J.; Lee, H.-J.; Park, J.-h.; Lee, Y.-B.; Kim, H. C.; Yoon, C. W.; Nam, S. W.; Kang, S. O. *J. Mater. Chem. A* **2013**, *1*, 1976-1981.
(18) Kaznatcheev, K. V.; Karunakaran, C.; Lanke, U. D.; Urquhart, S. G.; Obst, M.; Hitchcock, A. P. *Nucl. Instr. Meth. Phys. Res. A* **2007**, *582*, 96-99.
(19) Jacobsen, C.; Wirick, S.; Flynn, G.; Zimba, C. *J. Microsc.* **2000**, *197*, 173-184.
(20) Henke, B. L.; Gullikson, E. M.; Davis, J. C. *At. Data Nucl. Data Tables* **1993**, *54*, 181-342.
(21) Zhou, J.; Wang, J.; Fang, H.; Wu, C.; Cutler, J. N.; Sham, T. K. *Chem. Commun.* **2010**, *46*, 2778-2780.
(22) Zhou, J. G.; Wang, J.; Liu, H.; Banis, M. N.; Sun, X. L.; Sham, T. K. *J. Phys. Chem. Lett.* **2010**, *1*, 1709-1713.
(23) Zhou, J. G.; Wang, J.; Fang, H. T.; Sham, T. K. *J. Mater. Chem.* **2011**, *21*, 5944-5949.
(24) Hod, O. *J. Chem. Theory Comput.* **2012**, *8*, 1360-1369.
(25) Iyer, G. R. S.; Wang, J.; Wells, G.; Guruvenket, S.; Payne, S.; Bradley, M.; Borondics, F. *ACS Nano* **2014**, *8*, 6353-6362.
(26) Stöhr, J. *NEXAFS Spectroscopy*; Springer, 1992.
(27) Ma, H.; Lin, S. H.; Carpenter, R. W.; Rice, P.; Sankey, O. F. *J. Appl. Phys.* **1993**, *73*, 7422-7426.
(28) Terauchi, M. *Microsc. Res. Tech.* **2006**, *69*, 531-537.
(29) Pacilé, D.; Papagno, M.; Skála, T.; Matolín, V.; Sainsbury, T.; Ikuno, T.; Okawa, D.; Zettl, A.; Prince, K. C. *J. Phys. Condens. Matter* **2010**, *22*, 295301.
(30) Petravic, M.; Peter, R.; Kavre, I.; Li, L. H.; Chen, Y.; Fan, L.-J.; Yang, Y.-W. *Phys. Chem. Chem. Phys.* **2010**, *12*, 15349-15353.
(31) Caretti, I.; Jiménez, I. *J. Appl. Phys.* **2011**, *110*, -.
(32) Liu, L.; Sham, T.-K.; Han, W.; Zhi, C.; Bando, Y. *ACS Nano* **2010**, *5*, 631-639.
(33) Liu, L.; Sham, T.-K.; Han, W. *Phys. Chem. Chem. Phys.* **2013**, *15*, 6929-6934.
(34) Bozanic, A.; Petravic, M.; Fan, L. J.; Yang, Y. W.; Chen, Y. *Chem. Phys. Lett.* **2009**, *472*, 190-193.
(35) Gao, S.-P.; Pickard, C. J.; Payne, M. C.; Zhu, J.; Yuan, J. *Phys. Rev. B* **2008**, *77*, 115122.
(36) Park, C.-H.; Spataru, C. D.; Louie, S. G. *Phys. Rev. Lett.* **2006**, *96*, 126105.